Electronic Supporting Information

Solid-State Synthesis of Stable and Color Tunable Cesium Lead Halide Nanocrystals and Mechanism of High-Performance Photodetection in Monolayer $MoS_2/CsPbBr_3$ Vertical Heterojunction

Joydip Ghosh[1], Larionette P. L. Mawlong[2], Manasa G. B[3], Alexander J. Pattison[4],

Wolfgang Theis[4], Sudip Chakraborty[3] and P. K. Giri[1, 2*]

[1]*Department of Physics, Indian Institute of Technology Guwahati, Guwahati - 781039, India*
[2]*Centre for Nanotechnology, Indian Institute of Technology Guwahati, Guwahati - 781039, India*
[3]*Discipline of Physics, Indian Institute of Technology Indore, Simrol, Indore - 453552, India*
[4]*Nanoscale Physics Research Laboratory, School of Physics and Astronomy, University of Birmingham, Birmingham B15 2TT, UK*

S1.1 Characterization Techniques

The morphology and structural properties of as-grown $CsPbX_3$ NCs were analyzed using field emission transmission electron microscope (FETEM) (JEOL-2100F) including high-resolution TEM (HRTEM) operated at 200 kV. High-angle annular dark-field scanning TEM (HAADF-STEM) and corresponding energy-dispersive X-ray spectroscopy (EDS) of NCs were performed using an aberration-corrected STEM (JEM 2100F, 200 kV). X-ray diffractometer (XRD) (Rigaku RINT 2500 TRAX−III, Cu Kα radiation) was used for the determination of phase and structure of

---

* Corresponding authors, email giri@iitg.ac.in (PKG), sudiphys@gmail.com, sudip@iiti.ac.in (SC)

different $CsPbX_3$ NCs. X-ray photoelectron spectroscopy (XPS) measurements were performed with a PHI X-Tool automated photoelectron spectrometer (PHI X-tool, ULVAC-PHI Inc.) using Al K_α X-ray beam (1486.6 eV) with a beam current of 5 mA. Bruker Innova atomic force microscope (AFM) was used in tapping mode for the examination of the topography of the CVD grown MoS_2 layer. Further, Bruker EFM (electrostatic force microscopy) toolkit with probe carrier and sample holder enabled with biasing leads was utilized for KPFM measurement to estimate the work function of 1L-MoS_2 and 1L-MoS_2/$CsPbBr_3$ heterojunction. For the KPFM measurement, conducting platinum (Pt)/ iridium (Ir)-coated tips with an optimum frequency~72 kHz was used. The measurements were performed in the dual-pass lift mode in order to avoid noise and cross-talk between the topography and the surface potential measurement. UV–Vis absorption and diffuse reflectance measurement were carried out using a commercial spectrophotometer (PerkinElmer, Lamda 950). A commercial fluorimeter (Horiba Jobin Yvon, Fluoromax-4) was used for the measurement of the room temperature steady-state PL of different samples. The PL QY of different $CsPbX_3$ NCs samples was obtained by using an integrating sphere (FM-SPHERE, Horiba) attached to the fluorimeter. Temperature-dependent (80–300 K) PL measurements were performed under vacuum using a liquid nitrogen-cooled optical cryostat (Optistat DNV, Oxford Instruments). Time-resolved PL (TRPL) decay spectra of the different samples were recorded using a 375 nm pulsed laser excitation (average power ∼1.0 mW), with an instrument time response of <50 ps (LifeSpecII, Edinburgh Instruments). The temporal response of the photocurrent and I-V measurement of the PDs were carried out using a microprobe station (ECOPIA EPS-500), a 405 nm laser with TTL modulation and a source meter (Keithley 2400). The spectral photoresponsivity of the PD was measured using a Xenon lamp (Newport) with a manual monochromator (Newport), and a source meter (Keithley 2400).

S1.2 Computational Methodology

In order to envisage the hidden electronic structure and the charge transfer mechanism of the $MoS_2/CsPbBr_3$ composite system, we have performed systematic electronic structure calculations within the framework of density functional theory (DFT). The individual systems and their composite have been optimized through ionic relaxation to attain the minimum energy configurations. After finding the relaxed optimized structures of all the considered systems, the projected density of states and charge density have been determined using Vienna Ab-initio Simulation Package (VASP) code, where projector augmented wave (PAW) formalism is implemented. Throughout our calculations, we have used General Gradient Approximation (GGA) approach as implemented in Predew-Burke-Ernzerhof (PBE) functional to treat the exchange and correlation energies. The converged energy cut-off used throughout the calculation has been set at 500 eV. The Brillouin zone has been sampled using 3×3×1 Monkhorst-Pack k-mesh for the ionic relaxation in case of MoS_2 and $MoS_2/CsPbBr_3$ systems, whereas it has been sampled using 1×1×1 Gamma point in case of $CsPbBr_3$ NCs. We have kept adequate vacuum along Z-axis in order to nullify the interaction between the periodic images of the surface system. One of the prime focus of this investigation is the charge transfer mechanism between MoS_2 and $CsPbBr_3$ NCs. In order to explore the possible charge transfer between the surface and NCs system, we have obtained charge density distribution of the composite system, while doing self-consistent electronic structure calculation.

Table S1: Details of the fitting parameters of time resolved PL decay for different $CsPbX_3$ NCs.

Sample	τ_1 (ns)	A_1 (%)	τ_2 (ns)	A_2 (%)	τ_3 (ns)	A_3 (%)	τ_{ave} (ns)
$CsPbCl_3$	0.6	8.6	5.2	54.4	17.5	37.0	13.7
$CsPbCl_{1.5}Br_{1.5}$	2.2	16.2	6.4	61.8	22.8	22.1	15.0
$CsPbBr_3$	2.3	6.8	4.9	49.4	22.3	43.8	18.6
$CsPbBr_{1.5}I_{1.5}$	1.0	8.6	9.1	38.3	36.1	53.1	31.8
$CsPbI_3$	0.8	0.8	13.9	6.4	101.7	92.8	100.9

Table S2: Comparison of the performance of the 1L-MoS_2/$CsPbBr_3$ photodetector with reported $CsPbBr_3$ based photodetectors.

Device	Device structure	Incident light (wavelength/ intensity)	Rise time/fall time	Responsivity (A/W)	Detectivity (Jones)	Reference
$CsPbBr_3$/Au NC	-	532 nm/ 4.65 mW cm^{-2}	0.2 ms /1.2 ms	0.01004	4.56×10^{8}	[1]
$CsPbBr_3$ nanonet film	-	473 nm/ 1.45 μW cm^{-2}	11 ms/ 16 ms	2.84	5.47×10^{12}	[2]
$CsPbBr_3$ Single Crystal	-	450 nm, -	<100 ms	0.028	-	[3]
$CsPbBr_3$ Microplatelets	-	405/ 1 μW	20.9 ms/ 24.6 ms	1.33	0.86×10^{12}	[4]
$CsPbBr_3$ microparticles	-	-	1.8 ms/ 1.0 ms	0.18	6.1×10^{10}	[5]
MoS_2/$CsPbBr_3$ nanosheets	planar	442 nm/ 20 μW cm^{-2}	0.72 ms/ 1.01 ms	4.4	2.5×10^{10}	[6]
MoS_2/$CsPbBr_3$ QDs	FET	405 nm/ 12.8 μW cm^{-2}	7.5 ms/ 8 ms	4.68×10^{4}	-	[7]
WS_2/$CsPbBr_3$ nanowire	planar	450 nm/ ~40 nW	~2 ms/ 2 ms	57.2	1.36×10^{14}	[8]
MoS_2/$CsPbBr_3$ NCs	vertical	405 nm/ 0.6 mW cm^{-2}	5.5 μs/ 24 μs	24.34	3.93×10^{12}	*This study*

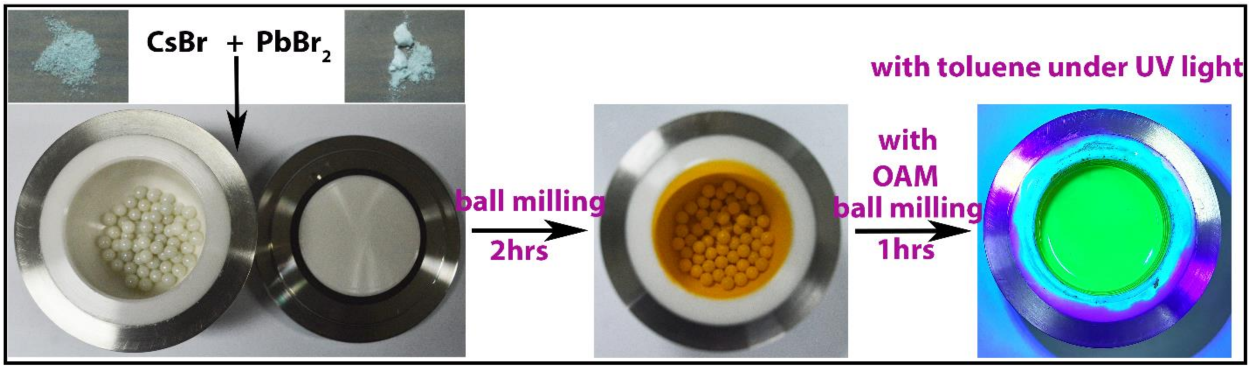

Fig. S1: Photographs of the solid-state synthesis steps of all inorganic perovskite NCs by ball milling method.

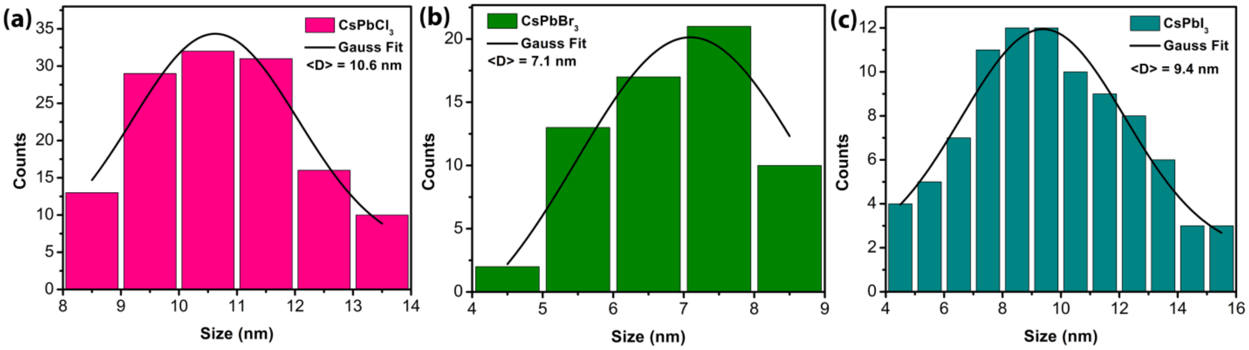

Fig. S2: Size distributions of (a) $CsPbCl_3$ NCs, (b) $CsPbBr_3$ NCs (c) $CsPbI_3$ NCs. The solid line in each case shows the corresponding Gaussian fitting and <D> indicates the average size of the NCs.

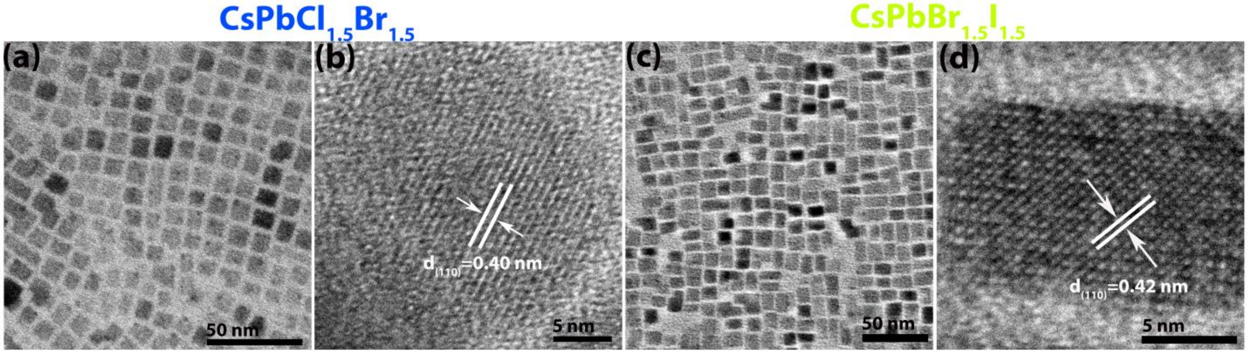

Fig. S3: TEM image and HRTEM lattice fringe image of (a, b) $CsPbCl_{1.5}Br_{1.5}$ NCs, (c, d) $CsPbBr_{1.5}I_{1.5}$ NCs.

.

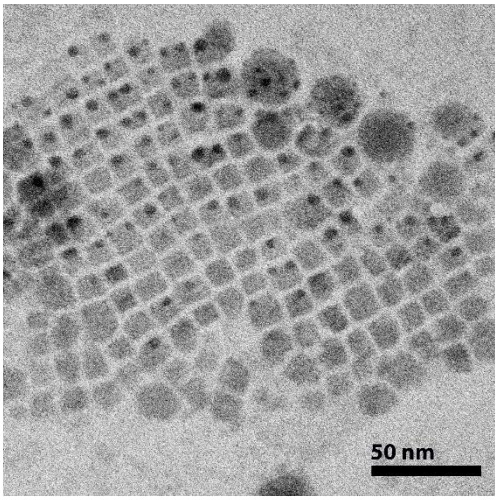

Fig. S4: TEM image of $CsPbBr_3$ NCs synthesized by a single-step OMA assisted milling.

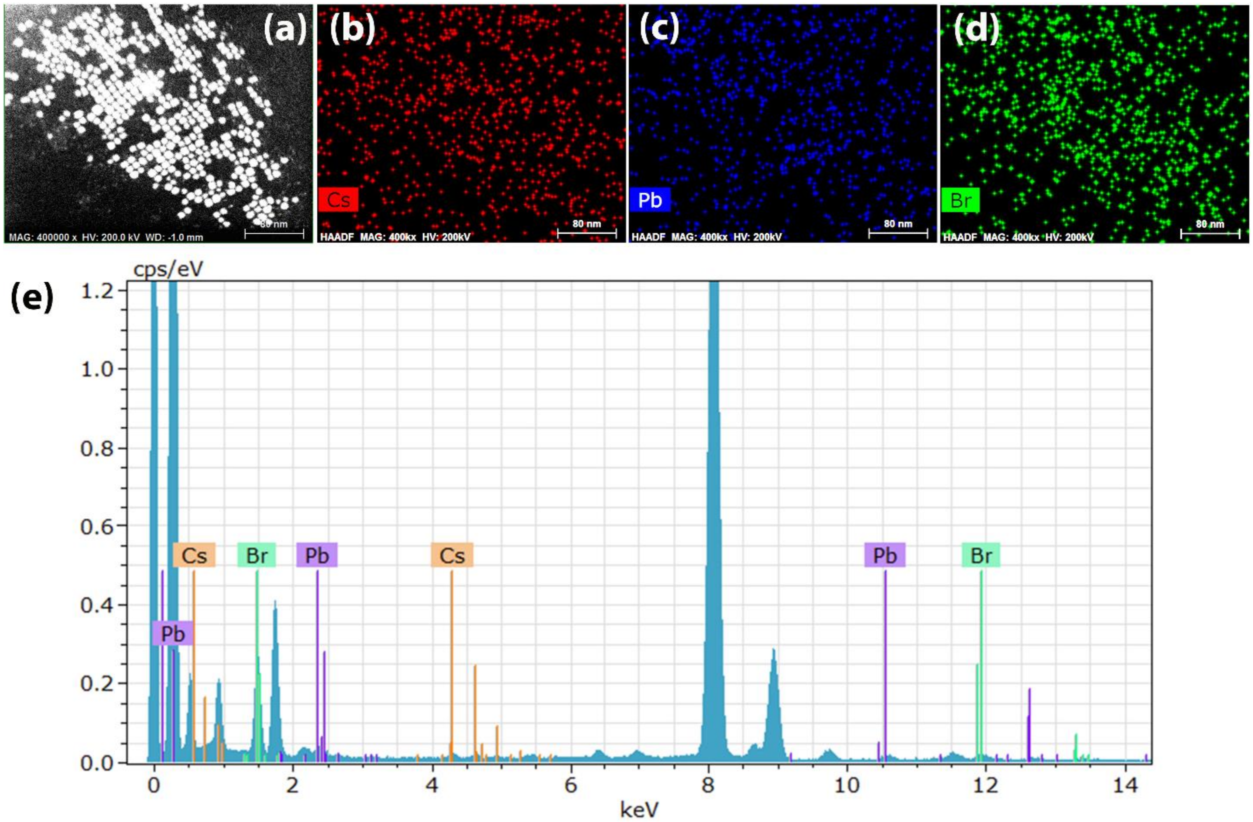

Fig. S5: (a-d) HAADF image and EDS elemental color mapping of Cs, Pb and Br, respectively. (e) EDX spectra of $CsPbBr_3$ NCs.

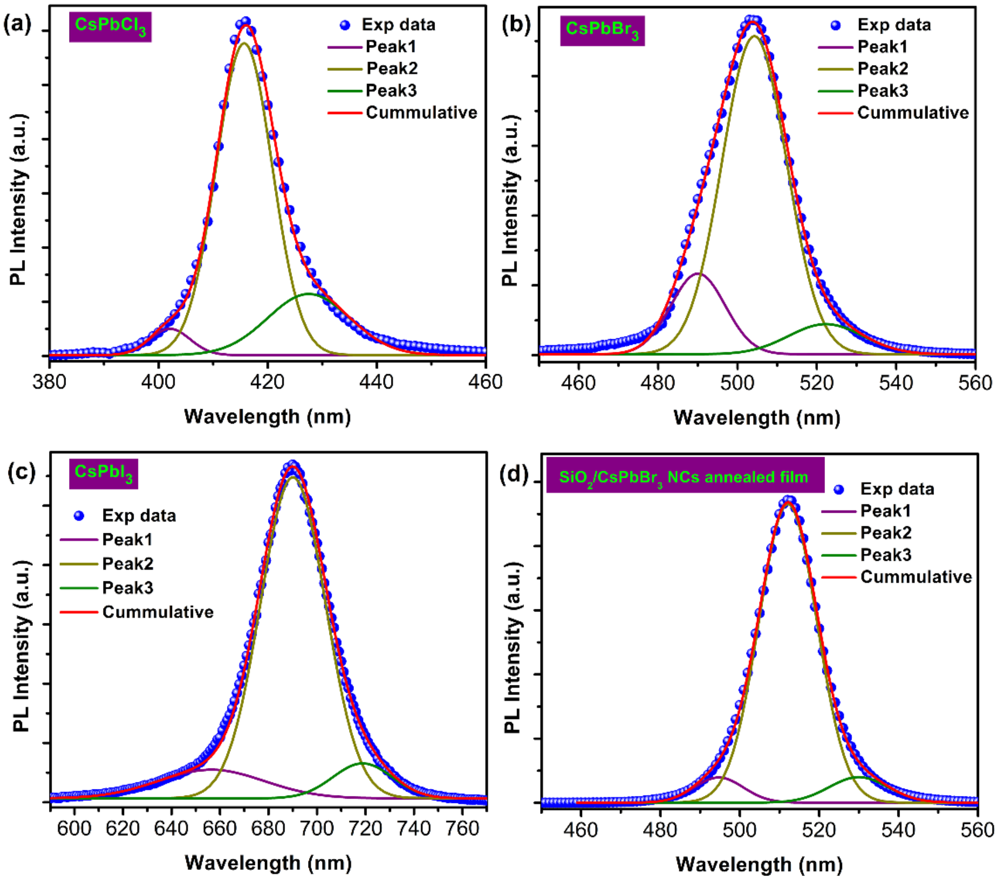

Fig. S6: Gaussian deconvolution of the PL spectra with three peaks in each case for (a) $CsPbCl_3$ NCs, (b) $CsPbBr_3$ NCs, (c) $CsPbI_3$ NCs, and (d) $CsPbBr_3$ NCs film after annealing at 80 °C for 15 min.

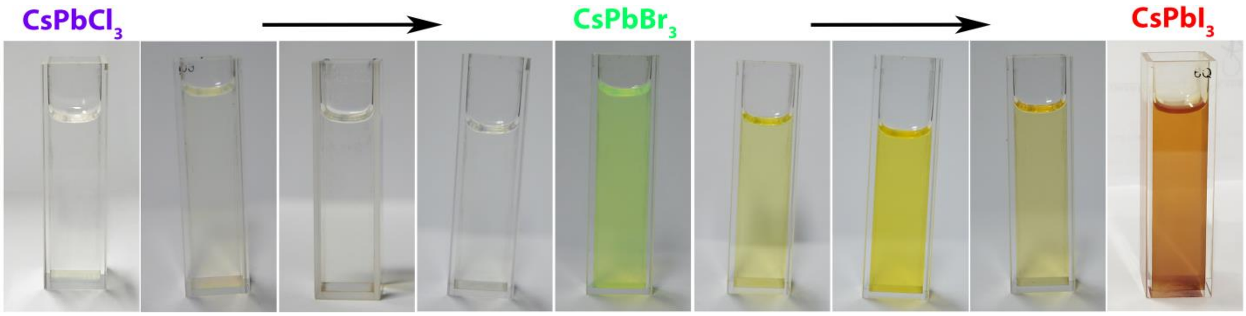

Fig. S7: Photographs of the colloidal dispersions of $CsPbX_3$ NCs in toluene under room light.

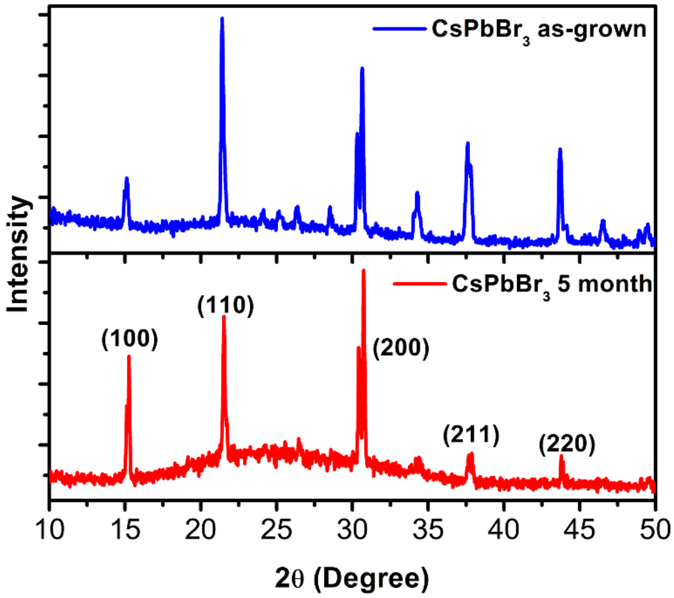

Fig. S8: Comparison of the XRD pattern of as-grown and after 5 months of storage of $CsPbBr_3$ NCs in ambient conditions.

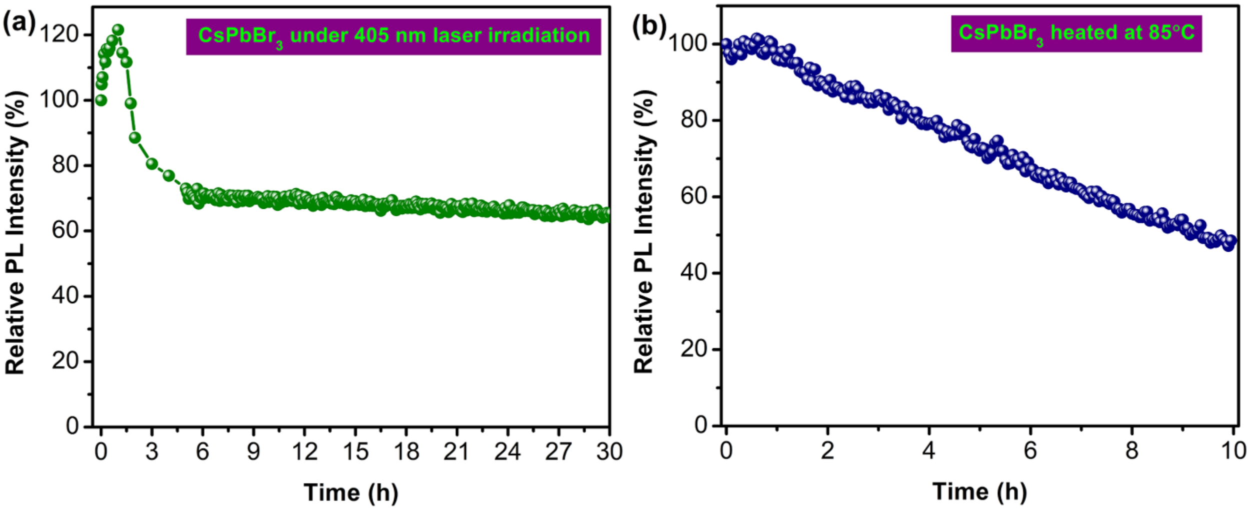

Fig. S9: (a) PL intensity of $CsPbBr_3$ NCs film as a function of laser exposure time under continuous irradiation of 405 nm CW laser. (b) Change in PL intensity with heating time of $CsPbBr_3$ NCs film heated at 85° C.

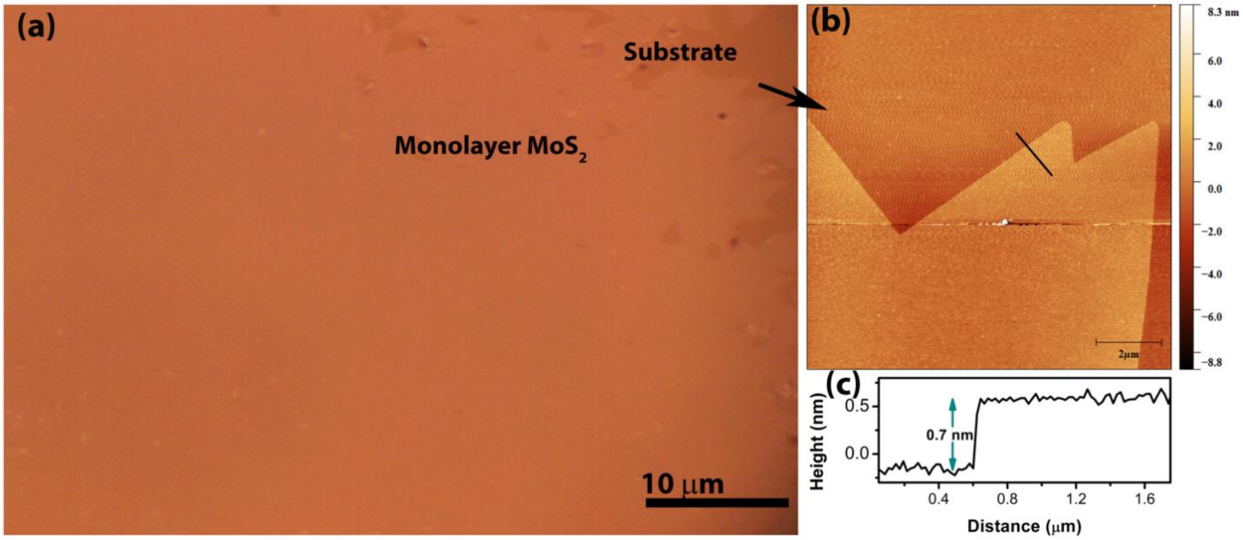

Fig. S10: (a) Optical microscope image of large area 1L- MoS_2 layer grown on Si/SiO_2 by direct CVD technique. (b) AFM image of 1L-MoS_2 on Si/SiO_2 substrate. (c) AFM height profile of 1L-MoS_2.

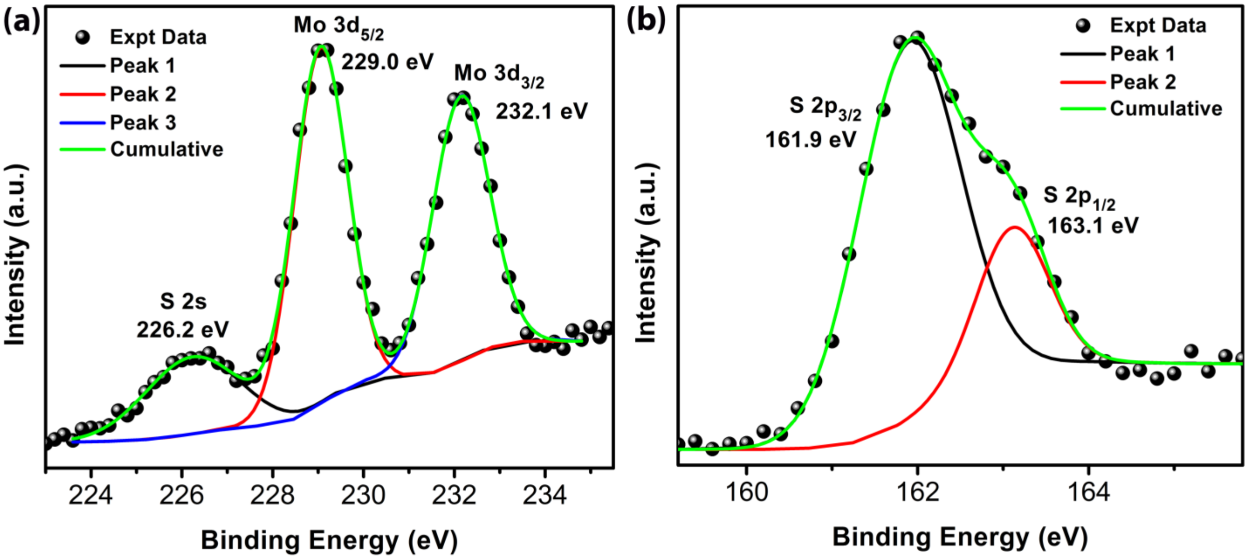

Fig. S11: Core level XPS spectra of (a) Mo 3d and (b) S 2p for 1L-MoS_2. The symbols are experimental data and the solid lines are Gaussian fittings.

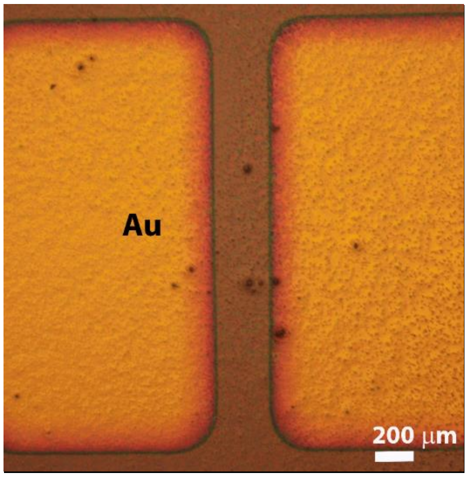

Fig. S12: Optical microscope image of the Au electrodes in the heterojunction photodetector.

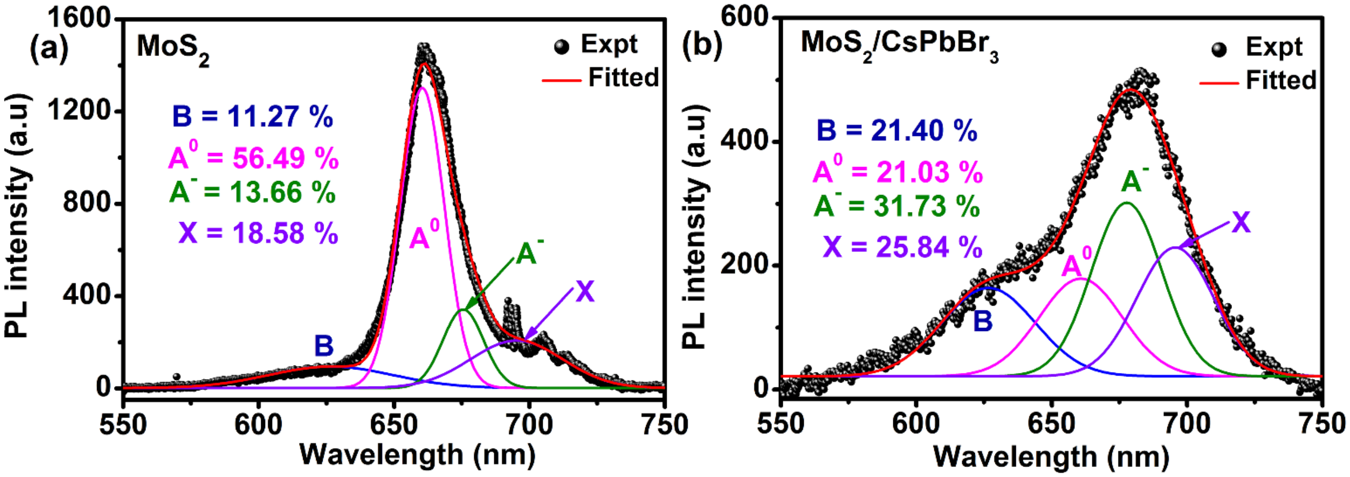

Fig. S13: Gaussian deconvolution of the PL spectra of (a) the pristine 1L-MoS_2 and (b) 1L-$MoS_2/CsPbBr_3$ NCs heterostructure.

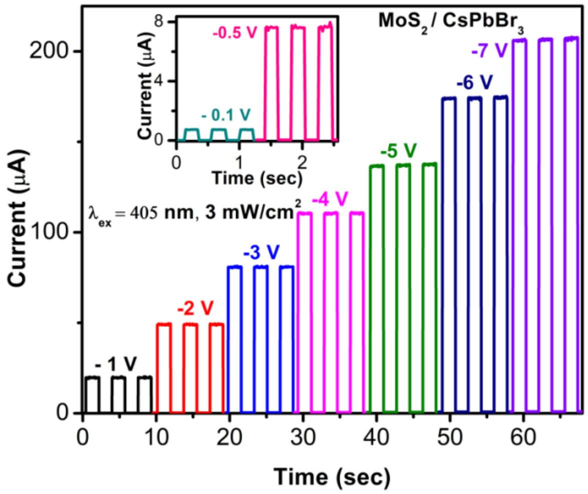

Fig. S14: Transient response of the photocurrent in 1L-MoS$_2$/CsPbBr$_3$ NC vertical heterojunction photodetector at different applied biases under the illumination of 405 nm laser of intensity 3 mW/cm^2.

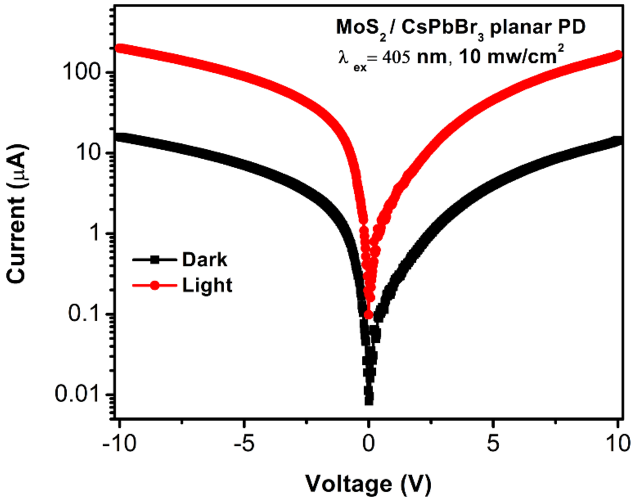

Fig. S15: I-V characteristics of MoS$_2$/CsPbBr$_3$ photodetector with planar contact structure.

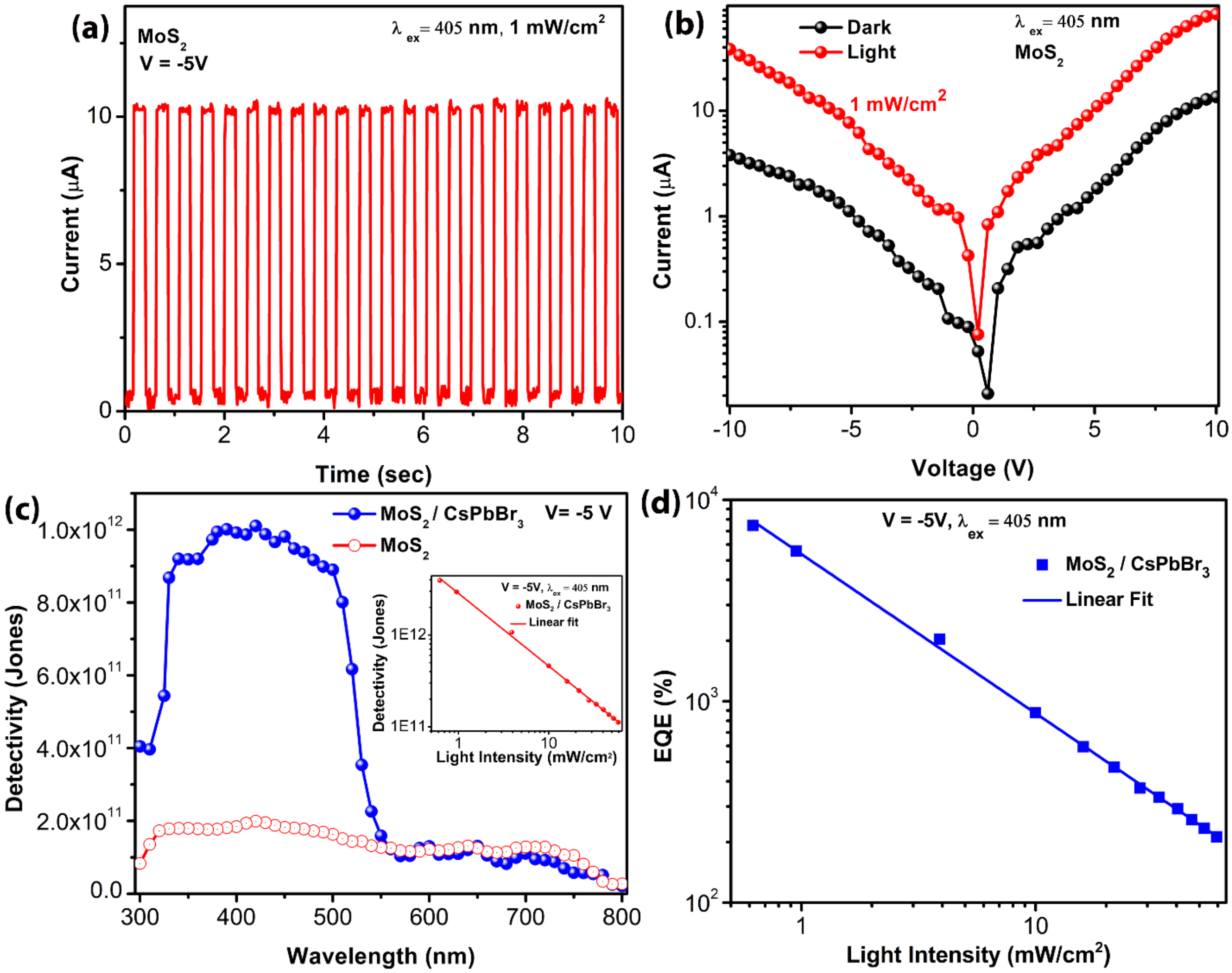

Fig. S16: (a) Transient response of the photocurrent in pristine 1L-MoS$_2$ photodetector at 5V under 405 nm laser illumination (at 1 mW/cm^2). (b) I–V characteristics of the 1L-MoS$_2$ photodetector in the dark and under light (405 nm). (c) Spectral detectivity of 1L-MoS$_2$/CsPbBr$_3$ and MoS$_2$ photodetector in the wavelength 300-800 nm at 5V. The inset shows the detectivity of the hybrid PD as a function of incident light intensity. (d) EQE of 1L-MoS$_2$/CsPbBr$_3$ heterojunction PD as a function on incident light intensity.

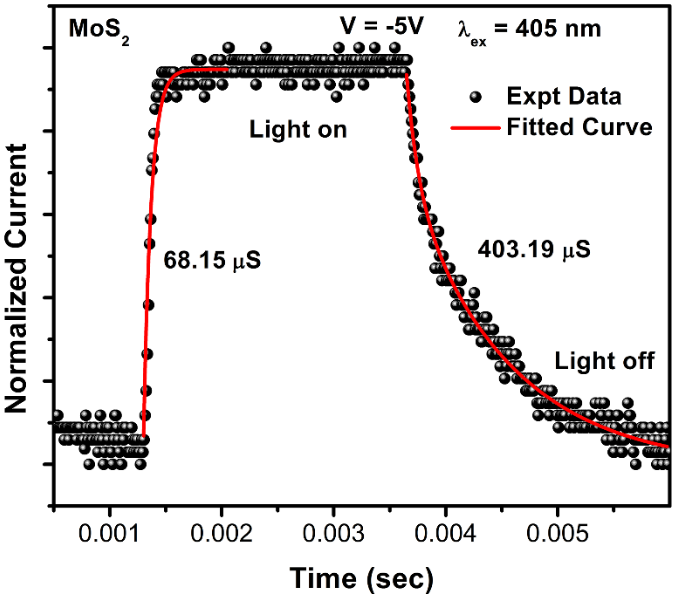

Fig. S17: Transient response of the photocurrent in bare MoS_2 photodetector with exponential fit for the growth and decay of photocurrent.

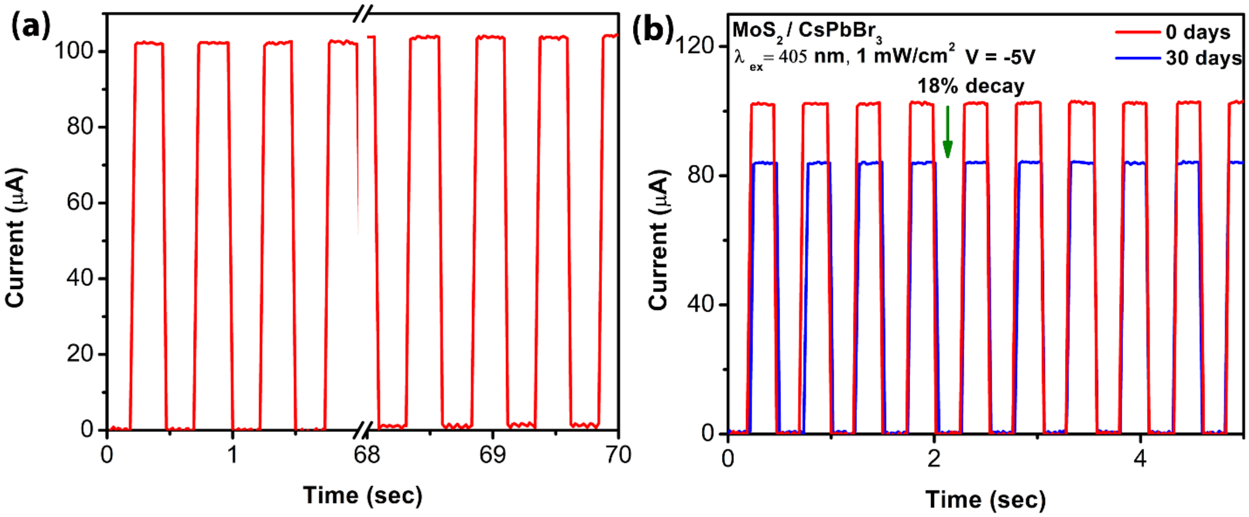

Fig. S18: (a) Time-dependent photocurrent response of 1L-MoS_2/$CsPbBr_3$ NC heterojunction photodetector showing minor change in photocurrent due to the light soaking. (b) Comparison of time-dependent photocurrent response of as-grown 1L-MoS_2/$CsPbBr_3$ heterojunction photodetector and after 10 days of storage in ambient condition.

References:

1. Y. Dong, Y. Gu, Y. Zou, J. Song, L. Xu, J. Li, J. Xue, X. Li and H. Zeng, *Small*, 2016, **12**, 5622-5632.
2. R. Liu, H. Zhou, Z. Song, X. Yang, D. Wu, Z. Song, H. Wang and Y. Yan, *Nanoscale*, 2019, **11**, 9302-9309.
3. J. Ding, S. Du, Z. Zuo, Y. Zhao, H. Cui and X. Zhan, *The Journal of Physical Chemistry C*, 2017, **121**, 4917-4923.
4. Y. Li, Z. Shi, L. Lei, F. Zhang, Z. Ma, D. Wu, T. Xu, Y. Tian, Y. Zhang, G. Du, C. Shan and X. Li, *Chemistry of Materials*, 2018, **30**, 6744-6755.
5. X. Li, D. Yu, F. Cao, Y. Gu, Y. Wei, Y. Wu, J. Song and H. Zeng, *Advanced Functional Materials*, 2016, **26**, 5903-5912.
6. X. Song, X. Liu, D. Yu, C. Huo, J. Ji, X. Li, S. Zhang, Y. Zou, G. Zhu, Y. Wang, M. Wu, A. Xie and H. Zeng, *ACS Applied Materials & Interfaces*, 2018, **10**, 2801-2809.
7. R. Lin, X. Li, W. Zheng and F. Huang, *ACS Applied Nano Materials*, 2019, **2**, 2599-2605.
8. Q. Xu, Z. Yang, D. Peng, J. Xi, P. Lin, Y. Cheng, K. Liu and C. Pan, *Nano Energy*, 2019, **65**, 104001.